Brain Structure and Function
https://doi.org/10.1007/s00429-018-1725-y

ORIGINAL ARTICLE

Fast prenatal development of the NPY neuron system in the neocortex of the European wild boar, *Sus scrofa*

Laura Ernst[1] · Simon Darschnik[1] · Johannes Roos[2] · Miriam González-Gómez[3] · Christa Beemelmans[4] · Christoph Beemelmans[4] · Maren Engelhardt[2] · Gundela Meyer[5] · Petra Wahle[1]

Received: 6 March 2018 / Accepted: 26 July 2018

Abstract

Knowledge on cortical development is based mainly on small rodents besides primates and carnivores, all being altricial nestlings. Ungulates are precocial and born with nearly mature sensory and motor systems. Almost no information is available on ungulate brain development. Here, we analyzed European wild boar cortex development, focusing on the neuropeptide Y immunoreactive (NPY-ir) neuron system in dorsoparietal cortex from E35 to P30. Transient NPY-ir neuron types including archaic cells of the cortical plate and axonal loop cells of the subplate which appear by E60 concurrent with the establishment of the ungulate brain basic sulcal pattern. From E70, NPY-ir axons have an axon initial segment which elongates and shifts closer towards the axon's point of origin until P30. From E85 onwards (birth at E114), NPY-ir neurons in cortical layers form basket cell-like local and Martinotti cell-like ascending axonal projections. The mature NPY-ir pattern is recognizable at E110. Together, morphologies are conserved across species, but timing is not: in pig, the adult pattern largely forms prenatally.

Keywords Transient neuropeptide Y neurons · NeuN · Glutamate decarboxylase · Gyration · Body and organ weight

Introduction

Knowledge on cortical development is based mainly on data from small rodents and, to a lesser extent, from cat, ferret and primates including human, all being altricial nestlings. By contrast, ungulates are precocial, born with nearly mature sensory and motor systems, and are immediately mobile. Almost no information is available on ungulate brain development, despite the pig being an important model for human diseases. Body mass, organ size, and physiology, e.g., of the immune system strongly resemble that of humans (Vodicka et al. 2005). Porcine and human neural stem cells feature similar properties and grow under the same conditions (Vodicka et al. 2005). The pig has been used to investigate brain trauma (Smith et al. 1999; Grate et al. 2003), developmental cerebral hypoxia–ischemia (Yue et al. 1997), prenatal effects of cytostatic agents and hypoglycemia (McGowan et al. 1995), retinal cell replacement (Klassen et al. 2012), ischemic stroke (Sakoh et al. 2001), and iPS therapies (Baker et al. 2017). Genetic models for Alzheimer's, Huntington's and Parkinson's disease, ALS, and spinal muscular atrophy are under development (Holm et al. 2016).

Electronic supplementary material The online version of this article (https://doi.org/10.1007/s00429-018-1725-y) contains supplementary material, which is available to authorized users.

✉ Petra Wahle
petra.wahle@rub.de

1 Developmental Neurobiology, Faculty of Biology and Biotechnology, Ruhr University Bochum, 44870 Bochum, Germany

2 Institute of Neuroanatomy, Medical Faculty Mannheim, CBTM, Heidelberg University, Heidelberg, Germany

3 Unit of Histology, Anatomy and Histology, Department of Basic Medical Science, Faculty of Medicine, University of La Laguna, 38200 Santa Cruz de Tenerife, Tenerife, Spain

4 Regionalverband Ruhr Grün, Forsthof Üfter Mark, Forsthausweg 306, 46514 Schermbeck, Germany

5 Unit of Histology, Department of Basic Medical Science, Faculty of Medicine, University of La Laguna, 38200 Santa Cruz de Tenerife, Tenerife, Spain

Published online: 09 August 2018

Pigs are cooperative animals with individual personalities (Friel et al. 2016) which can easily be trained on conditioning tasks (Gieling et al. 2011). In contrast to human or rodent infants (Dilger and Johnson 2010; Mudd and Dilger 2017), behavior can be assessed immediately after birth, since for instance, in wild boar, olfaction develops prenatally (Fulgione et al. 2017). Piglets learn by observing elders and have good long-term memory (Veit et al. 2017). Altogether, the pig is an emerging translational model filling the gap between studies in rodents and clinical trials in humans (Vodicka et al. 2005; Mudd and Dilger 2017).

Exploration of the pig CNS began decades ago in anatomical studies, followed by physiological and hodological studies locating somatosensory, motor, frontal, auditory, and visual cortex (Lind et al. 2007). The pig is gyrencephalic and resembles the human brain in terms of anatomy and development more than brains of commonly used small laboratory animals do (Lind et al. 2007). Developmental changes in fatty acid accretion parallel those of humans, and the gray matter/white matter (GM/WM) ratio as well as the gyration index is similar to human (Sweasey et al. 1976; Pond et al. 2000; Mudd and Dilger 2017). Stereotaxic atlases, PET and MRI imaging data exist to guide surgery and characterize transmitter systems (Lind et al. 2007). Longitudinal MRI data in domestic pig and human reveal similar growth trajectories with 1 week of pig brain volume growth being equal to 1 month of human infant brain development (Mudd and Dilger 2017). However, one has to take into account the detrimental effects of domestication (Kruska 1970; Lahvis 2017) resulting in an average reduction of the total brain weight in domestic pig by about 41% compared to wild boar (Böndel 2017).

Yet, little information exists on early pig brain development at the cellular level. From the forest to the lab: our goal is to characterize cortex development of a precocial ungulate at the cellular level, and the European wild boar, *Sus scrofa* (LINNAÈUS 1785), was our 'breed' of choice. Here, we characterized the early appearing neuropeptide Y (NPY) neuron system in cortical plate and subplate. It is to our knowledge, the first study on fetal brain development at the cellular level in a non-domesticated, non-captive, large-brained ungulate which is—according to folk wisdom—extremely smart.

Results

External appearance and developmental trajectories

The external features of the fetuses are shown in Online resource 2. Pigment is seen in the eye at E35. Toes are present at E45, and hooves at E60. The cusps of the canini have emerged in mandible and maxilla at E65/E70, and skin pigmentation is evident at the chin. At E60, a chin wart is present, sprouting black chin hair until E70. Skin pigmentation starts at E70 and more is present at E85 at snout, mandible, head, legs and feet. Hair is present at the eye brows from E85 onwards, and eyes become surrounded by eyelashes. The typical black and tan stripes of boar piglets are present at E100 and older, with fine black and brown hair covering head, face, back, and flanks. Canini and first incisivi are present in maxilla and mandible. The same tooth pattern is present at E110, and the cusps of next-emerging teeth can be recognized, but are still covered by epidermis. The features match the description of Henry (1968a). From E45 onwards, the skull bones become increasingly well vascularized, and blood vessels are present in the meninges already at E45. The dura mater becomes successively harder and difficult to cut at the falx cerebri and tentorial membrane.

Fetal measures are shown in Online resource 3. Curves for body weight, crown–rump length, and the weights of heart, lung, liver, kidney (average), spleen, and gastrointestinal tract (with stomach and gut not emptied) reveal a more or less linear increase until E110. Lung weight increases steeper towards the latest fetal stage, presumably in preparation for birth. Body weights and developmental trajectories correspond well with reported data (Pond et al. 2000). The average gestational length in domesticated pig and wild boar is E114 (Henry 1968b). After birth, body and organ growth increase steeply.

Sulcal pattern

Dorsal views of the fetal and postnatal brains arranged to the same scale are shown in Fig. 1. An E70 brain is shown in lateral and ventral view. All brains have been subsequently sliced into blocks and cut coronally according to the vertical plane indicated in the E70 lateral view. The orientation matches the stereotaxic coordinates used for MRI imaging of neonatal and adult pigs (Andersen et al. 2005; Sauleau et al. 2009; Saikali et al. 2010; Conrad et al. 2014). The heads of E35 have been processed and cut in toto, therefore the E45 is the youngest brain presented here. Sulci are not yet recognizable at E35 and E45. Major sulci are well recognizable at E60. We follow the species-comparative approach (Brauer and Schober 1970) and identified in dorsal views of the hemispheres the basic pattern typical for ungulates (Nickel et al. 1991) consisting of the ansate sulcus, the coronal sulcus branching off the ansate around its rostro-lateral bend, the continuation of the ansate towards the temporal lobe, finally meeting the suprasylvian sulcus. Further, we identify the first paramedian sulcus delineating a substantially long paramedian gyrus rostral to the ansate sulcus as the cruciate sulcus. The E60 brain already displays a shallow fissure projecting from the rostral pole towards

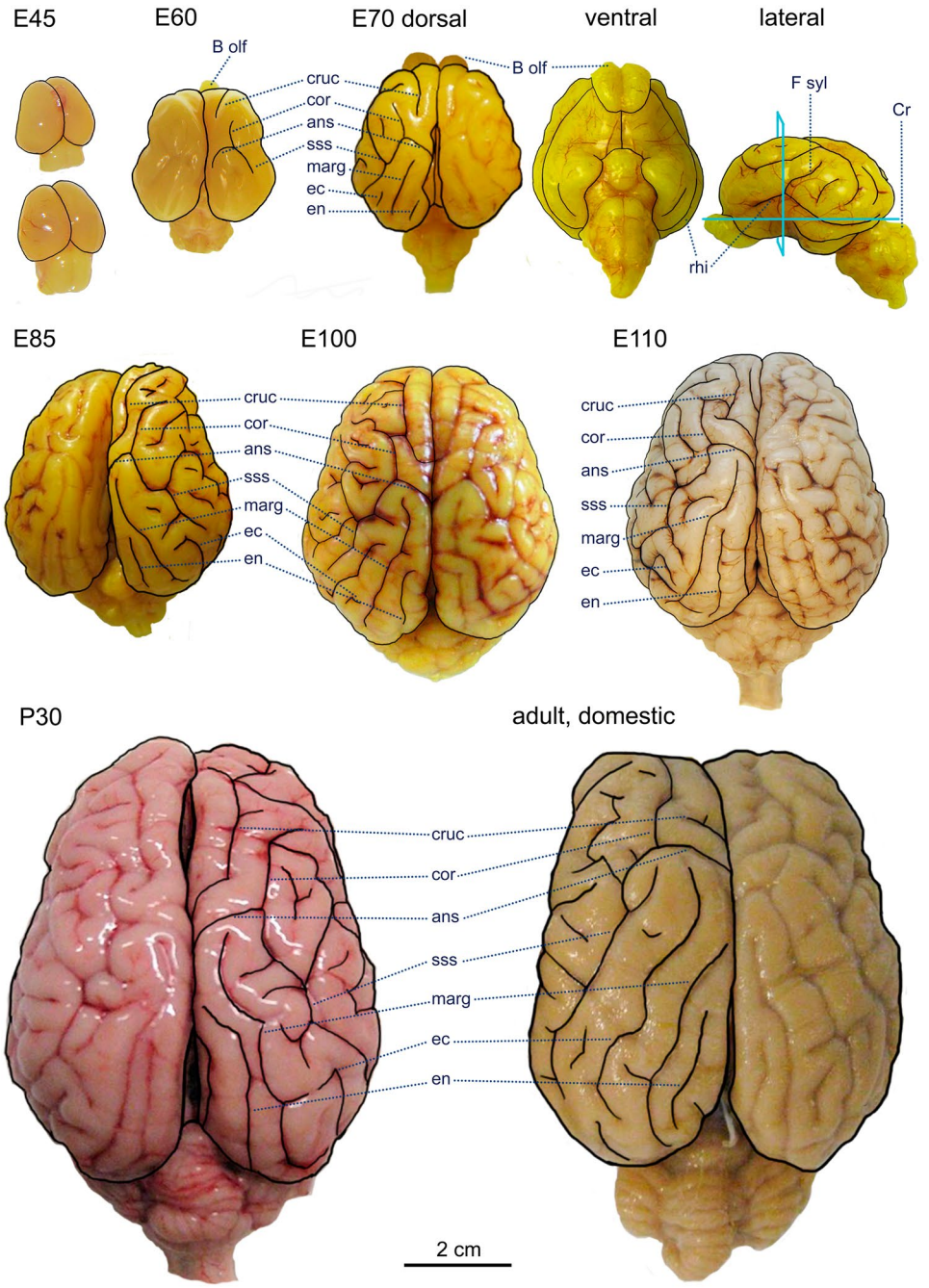

Fig. 1 Representative brain stages. Dorsal views of the brains at the ages examined with major sulci labeled (earliest at E60). The youngest stage, E35, is not shown as its head was processed in toto for paraffin embedding. Major sulci are highlighted by black lines in one hemisphere. ans, ansate sulcus; B olf, olfactory bulb; cor, coronal sulcus; Cr, cerebellum; cruc, cruciate sulcus; E, embryonic/fetal day; ec, ectomarginal sulcus; en, endomarginal sulcus; F syl, sylvian fissure; marg, marginal sulcus; P, postnatal day; rhi, rhinal fissure; sss, suprasylvian sulcus. Brains E45, E60, E70, E85, E100 and E110 have been photographed during dissection and after a short exposure to fixative containing picric acid. Brain P30 has been photographed before immersion into fixative. The brain of the adult domestic pig from the Institute's collection has been photographed months after fixation. Scale for all 2 cm

the already formed ansate sulcus, and medial to the already formed coronal sulcus (Fig. 1), it has formed into the cruciate sulcus at E70. The cruciate sulcus is present in all older brains except for 1 out of 5 brains of the E100 litter (Online resource 4, brain no. 5). The sulcus is variable in length, may not always merge with the longitudinal fissure, and may individually form smaller sulci. The caudal pole is dominated by the marginal sulcus, which is paralleled by the endo- and ectomarginal sulci. In one of our cases, the entomarginal sulcus has been more prominent than the marginal sulcus (Online resource 4, brain no. 3). Together, the pattern of major sulci can be recognized in the postnatal and all fetal brains down to E60, and is present in all five E100 brains. Additional minor sulci develop from E85 onwards with quite some variability between individuals and hemispheres.

Maturation of NPY-ir neurons

At all ages examined, NPY-ir is already expressed by very immature neurons migrating in the developing gray matter (GM) (Fig. 2a). We have assembled a serial longitudinal sequence of differentiation (Fig. 2b–e), which resembles that

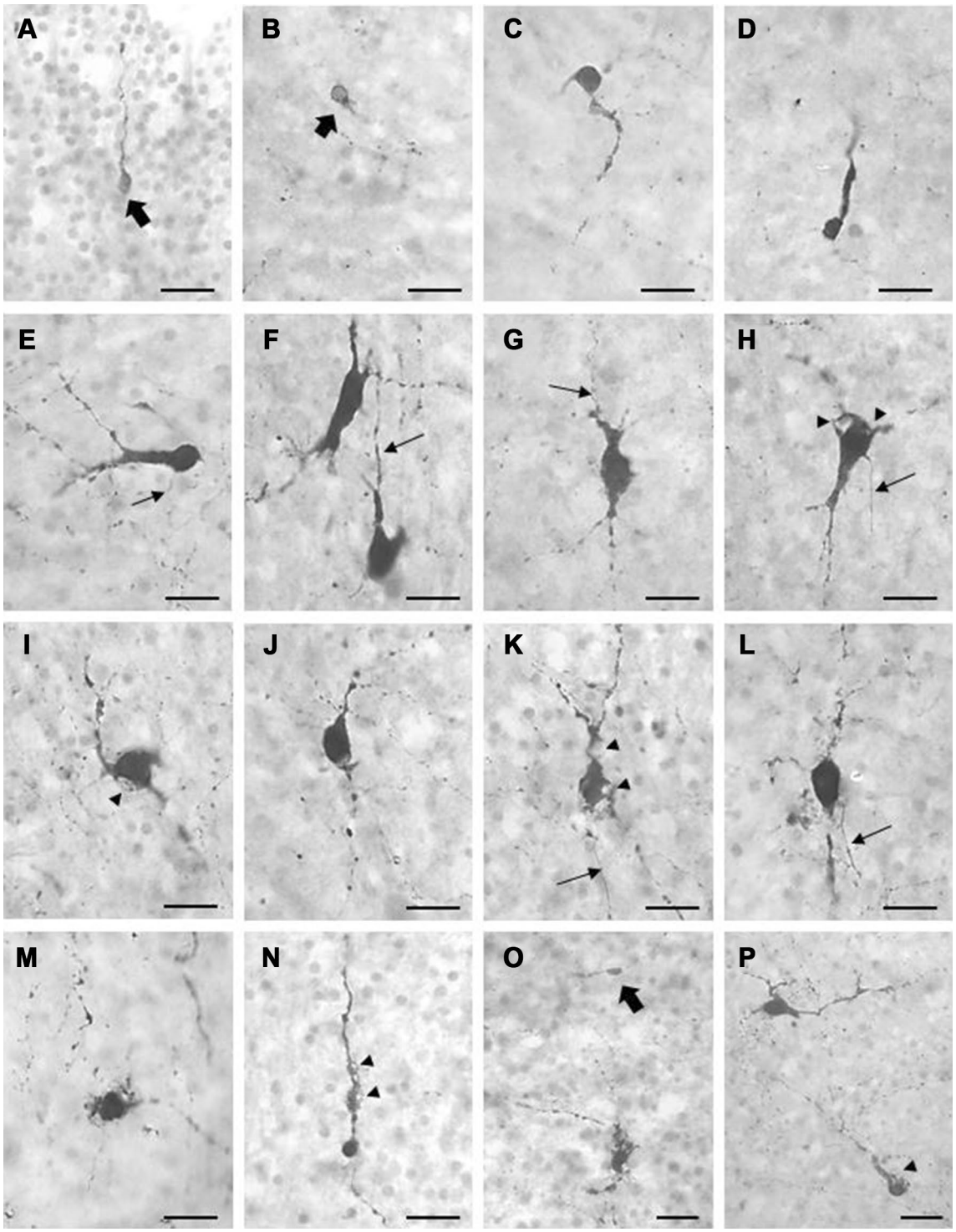

Fig. 2 Stages of cellular maturation and degeneration. **a** Migrating neuron in CP with a growth cone at the leading tip; E70. **b** Very immature neuron with tiny soma and marginal cytoplasm; E85, WM. **c, d** Slightly more mature neurons; E85 WM. **e** Larger soma with prominent branching dendrite; E85, layer VI. **f** Fully mature neurons with intact somata with a smooth outline; E85, layer VI. **g** Slightly shrunken soma; E85, WM. **h, i** Somata with vacuoles; E85, layer V and VI. **j** Shrunken soma with strongly beaded neurites; E85, layer V. **k** Shrunken soma and beaded neurites with vacuoles. **l** Neuron with fragmented dendrites; note that its intact axon passes microns near the break site. **m** Fragmented neuron; E85, WM. **n** Immature neuron with shrunken soma and swollen dendrite with vacuoles. **o** Heavily fragmented neuron next to a very immature soma (arrow); E70, layer VI. **p** Healthy mature neuron with intact soma in the same focal plane as a cell with vacuoles; E85, WM. Vacuoles indicated by arrowheads, axons indicated by fine arrows, immature somata indicated by bold arrows. **a**–**n** and **o**–**p** are at the same magnification to document the differences in soma sizes. Scale bars 25 μm

reported for kitten (Wahle and Meyer 1987). Fully mature multipolar to bitufted neurons with large somata and a smooth outline (Fig. 2g) give rise to long projecting and looping axons. Axonal loop neurons reside in the subplate/white matter (SP/WM), but also in the developing GM up to the marginal zone (MZ). Besides, intensely NPY-ir neurons can be found in various stages of degeneration with shrunken somata, varicose neurites, breaks in the somatic membrane and in dendrites, and vacuoles in somata and dendrites (Fig. 2g–l). Note in Fig. 2l that the intact axon of the affected neuron passes microns near a large dendritic break site; this argues against gross histological artifacts as a reason for the damage. The final stage of disintegration is an aggregation of ir-material, variable in shape (Fig. 2m). Disintegration can also affect immature neurons as indicated by small soma, large nucleus:cytosol ratio, and unipolar appearance (Fig. 2n). Immature, mature healthy-looking, and degenerating neurons occur close to each other in GM/WM (Fig. 2o, p). The same phenomenon has been observed at E70, E85, and E100, suggesting a heterochronic maturation and cell death not only in SP/WM, but also in GM.

Distribution and growth of NPY-ir somata

The distribution of NPY-ir somata has been plotted from E60–P30 in 10-µm-thick paraffin sections (Fig. 3). At E60, the majority of neurons reside in infragranular layers, but also in the cell-dense cortical plate and in the MZ. Surprisingly few are in the SP/WM at this age. At E70 and E85, numerous neurons are in GM and WM filling the space at near equal density despite a substantial size increase of the cortical sections. In addition, NPY-ir neurons and axons are scattered in the subventricular zone (SVZ) at E70 and E85 (Fig. 3). Many cells are immature at E60 and E70 (stages shown in Fig. 2a–d). These immature cells decline in number until E110. The percentages of immature neurons from all NPY-ir neurons (Fig. 3) are at E60: 53%, E70: 36.6%, E85: 23.6%, E100: 8.9%, and P30: 3.4%. Besides cellular degeneration, the decrease in overall cell density is likely due to the enormous expansion of the cortex causing a dilution of cells in the larger cortical volume until P30. We cannot exclude underestimation of numbers due to somatodendritic staining falling below detection limits.

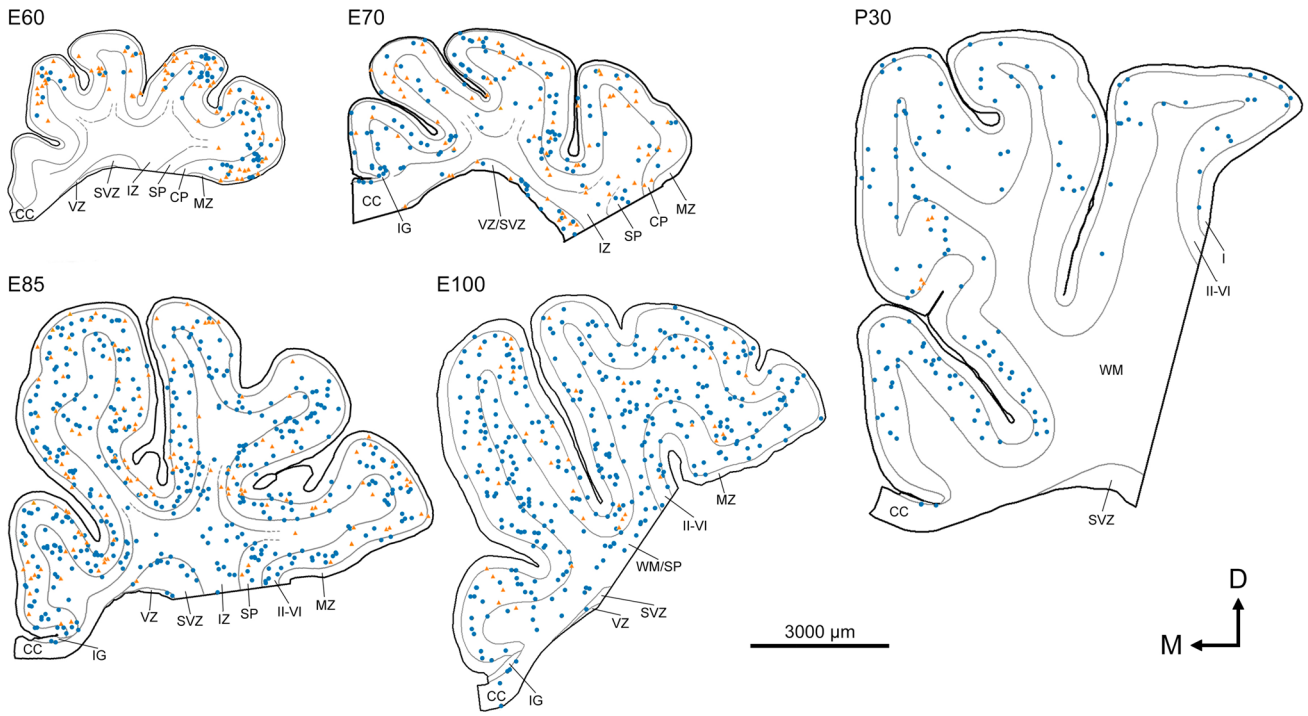

Fig. 3 Distribution of NPY-ir neurons from E60–P30. 10-µm-thick paraffin sections of dorsal cortex at the ages indicated have been used. Blue dots represent mature intensely labeled neurons (intact or degenerating), orange triangles represent immature neurons with weakly labeled small somata and/or unipolar morphology. Sections are taken mid-level rostral to the ansate sulcus and comprise cingulate, sigmoid and coronal gyrus, which display large layer V pyramidal neurons, and the somatosensory rostrum/face region lateral to the coronal sulcus with less prominent layer V pyramidal cells. Note that the scale does not exactly match the scale bars in the other figures, because the paraffin embedding shrinks fetal brains more than processing for cryostat sectioning. CC, corpus callosum; CP, cortical plate; IG, indusium grisium; IZ, intermediate zone; MZ, marginal zone; SP, subplate; SVZ, subventricular zone; VZ, ventricular zone; WM, white matter; I and II–VI, cortical layers. Scale bar 3 mm

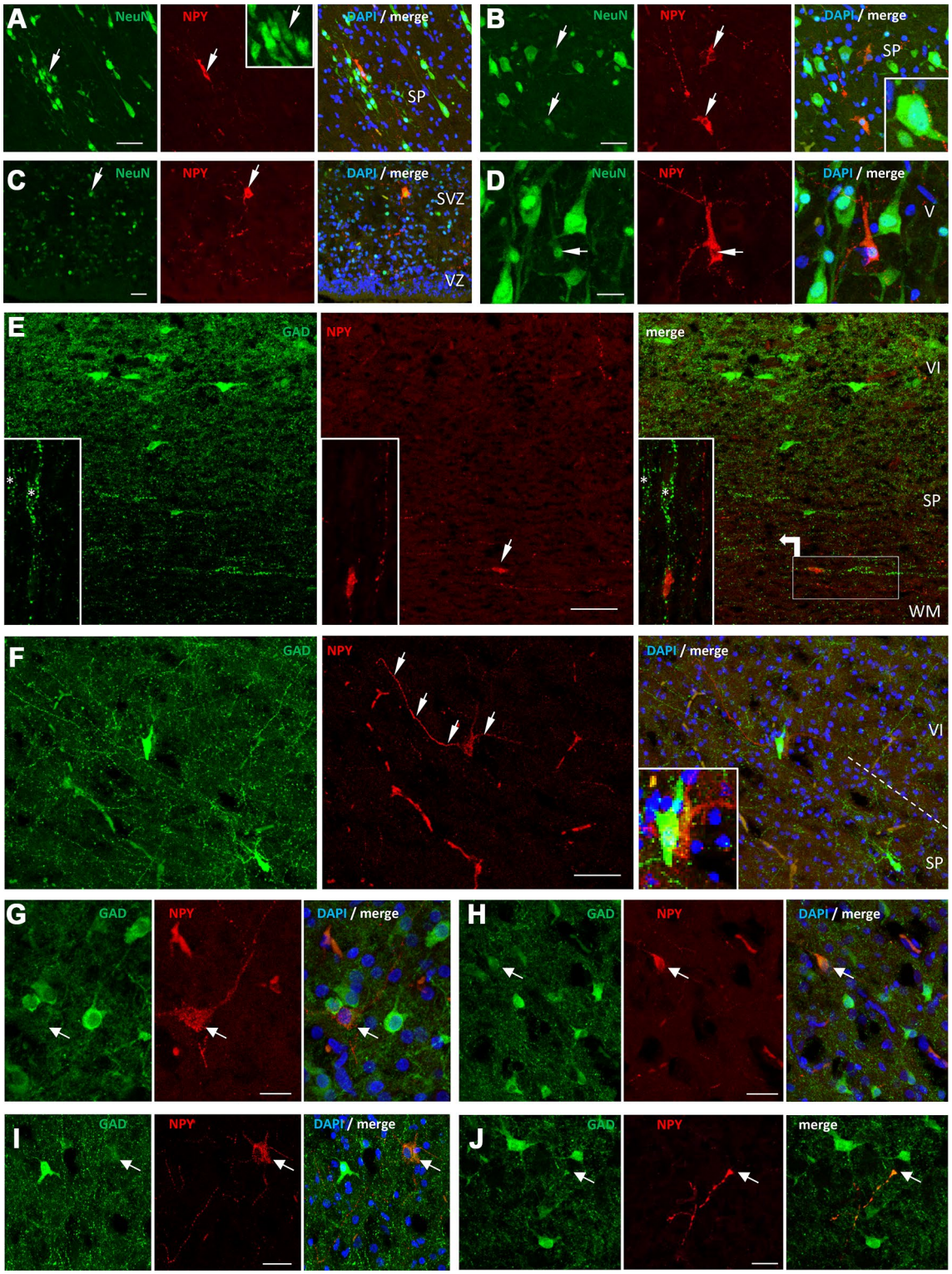

Substantial soma growth occurs in GM/MZ (Online resource 5A) with somata being small at E60 and E70 (mean with S.E.M., 68 ± 4.4 μm^2 and 68 ± 3.7 μm^2, resp.) due to many very immature NPY-ir neurons. Somata are larger at E85 (140 ± 11.4 μm^2), are even larger at E110 (189 ± 13.9 μm^2) and at P30 (241 ± 10.7 μm^2) due to decline of immature cells and increased numbers of mature NPY-ir neurons. NPY-ir neurons in SP/WM (Online resource 5B) are larger than those in GM/MZ from E70 onwards (76 ± 5.5 μm^2), with somatic area continuously increasing in size from

◂**Fig. 4** Neurochemical characterization of NPY-ir neurons at E85 and E100/110. **A** NPY-ir (red, arrow) and NeuN-ir (green) neurons in SP/WM at E85; inset shows the cluster of neurons at higher magnification. **b** NPY-ir (red, arrow) and NeuN-ir (green) neurons in SP/WM at E85; inset shows a NeuN-ir subplate neuron with NPY-ir boutons in close apposition. **c** NPY-ir and NeuN-ir neuron and NPY-ir axons in the SVZ at E85; fibers do not invade the VZ. **d** NPY-ir neurons among NeuN-ir layer V pyramidal cells at E110. Note the weak and mainly nuclear expression of NeuN-ir in NPY-ir neurons in comparison to the strong nuclear and cytosolic expression in neighboring neurons. Arrows point to double-labeled neurons; the merged picture has a DAPI counterstain. **e, f** GAD-65/67-ir neurons are present in GM and SP/WM at E85, as is a dense network of fibers and boutons. The boutons form clusters resembling basket-like terminals (**e**) around GAD-negative somata; boutons also occur in close apposition to NPY-ir somata (**e**, arrow; see enlargement of the boxed area, turned 90° counterclockwise). Note that NPY-ir neurons in SP/WM are GAD-negative (see insets in **e, f**; in **b**, arrows delineate the NPY-ir cell from blood vessel epithelia marked by autofluorescence in both channels). **g** Large NPY-ir, GAD-negative neuron in GM at E85. **h** NPY-ir, GAD-positive neuron in GM at E100. **i** NPY-ir, weakly GAD-positive neuron in GM at E110; note numerous basket-like terminals. **j** NPY-ir, GAD-positive axon with growth cone in GM at E100. Scale bars 25 µm in **a–d, c–f**, and 50 µm in **e, f**

E85 (151 ± 13.9 µm^2) to E110 (205 ± 17.6 µm^2) and to P30 (270 ± 16.2 µm^2).

Neurochemical characterization of NPY-ir neurons

NPY-ir cells coexpress the neuronal marker protein NeuN/RBFOX3 (Fig. 4a–d). Interestingly, at all ages and irrespective of position in SP/WM or GM, NPY-ir neurons display only a weak and mainly nuclear expression of NeuN. This differs clearly from the stronger nuclear and cytosolic expression in neighboring neurons, which are presumptive subplate pyramidal cells (Fig. 4a, b) or pyramidal cells of the GM (Fig. 4d). The proportion of NPY-ir from total neurons in the SP/WM is 2.49, 1.67, 1.69 and 0.81% at E70, E85, E100, and E110, respectively.

Neurons with looping axons have been identified with GAD staining in SP/WM of postnatal kitten (Wahle et al. 1987). In the adult mammalian cortex, NPY is colocalized in non-fast-spiking GABA-ergic neurons overlapping in distribution with somatostatin and calbindin (Markram et al. 2004; Qu et al. 2016). The neurons form boutons around somata and along dendrites (Wahle et al. 1986) in line with morphologies of small basket and Martinotti neurons. Thus, the assumption has been that NPY-ir neurons of SP/WM are GABA-ergic. In early postnatal rodent subplate, NPY-ir neurons colocalize somatostatin and nitric oxide synthase, typical markers of interneurons (Qu et al. 2016). In fetal wild boar, GAD-65/67-ir neurons occur in SP/WM, and there are numerous varicose axons some of which form basket-like terminals entwining large GAD-negative somata (Fig. 4a, inset). Unexpectedly, double-labeling of NPY-ir and GAD-65/67-ir at E85 and E100 reveals that the intensely NPY-ir neurons of SP/WM are GAD-negative (Fig. 4e, f). A quantification in several sections at E85 reveals 57 NPY-ir neurons and 180 GAD-ir neurons (ratio 1:3.2), but not a single double-labeled neuron. Further, the intensely NPY-ir axons and boutons in SP/WM and GM/MZ are void of GAD-ir (Fig. 4g), as are a number of large NPY-ir neurons in GM. At E85–E100, NPY-ir boutons are closely apposed to GAD-ir neurons suggesting axosomatic and axodendritic contacts (Online resource 6A, B). Vice versa, NPY-ir neurons of SP/WM (Fig. 4a) and GM/MZ are targeted by GAD-ir boutons; note that these NPY-ir neurons are also GAD-negative (Online resource 6C, D), indicating that NPY-ir and GAD-ir neurons are reciprocally wired. However, at E100, E110 and P30 many NPY-ir somata in GM/MZ are GAD-ir at variable intensity, and GAD-ir is found in growth cones of NPY-ir axons (Fig. 4h–j). This is the expected colocalization in the persisting interneurons.

NPY-ir fibers innervating pial blood vessels

The innervation arises from sympathetic neurons of the superior cervical ganglion, uses noradrenaline as main transmitter, and mediates vasoconstriction (Hamel 2006). In human, NPY-ir fibers along meningeal vessels seem to be present from gestational week 12 onwards (Kawamura et al. 1991). In boar, NPY-ir fibers are absent at E35 (not shown), but present along cerebral meningeal blood vessels from E45 onwards, which is weeks before the cortical neuron systems start to express NPY-ir (Online resource 7A, B). The coarse axons, often in bundles, have large varicosities and are thicker than the axons intrinsic to layer I (Online resource 7D, E). They run parallel to the vessels, likely small arteries (Online resource 7A, C, D, F, H, I), and freely in the meninges (Online resource 7G), but do not follow vessels descending into the cortex (Online resource 7J).

Distribution of NPY-ir axons

Thionin-staining reveals a broad MZ, as described for the domestic pig, containing reelin-ir neurons (Nielsen et al. 2010). Large layer V pyramidal neurons are easily detected at E70. A cell-dense cortical plate with small somata persists until E85. Layers have formed until E100 (Fig. 5). None or just one NPY-ir neuron is present per section at E45 and no axons are detectable. Substantial numbers of NPY-ir somata are present at E60 in the cortex and the MZ has numerous horizontal axons (Fig. 6a), many bearing growth cones (Fig. 6b–d). The density of fibers increases to highest level at P30, despite comparatively low numbers of NPY-ir somata at this age (Fig. 5). Long axons in WM and vertically ascending axons passing though the GM towards the MZ dominate younger stages, although horizontally and obliquely oriented axons are detectable

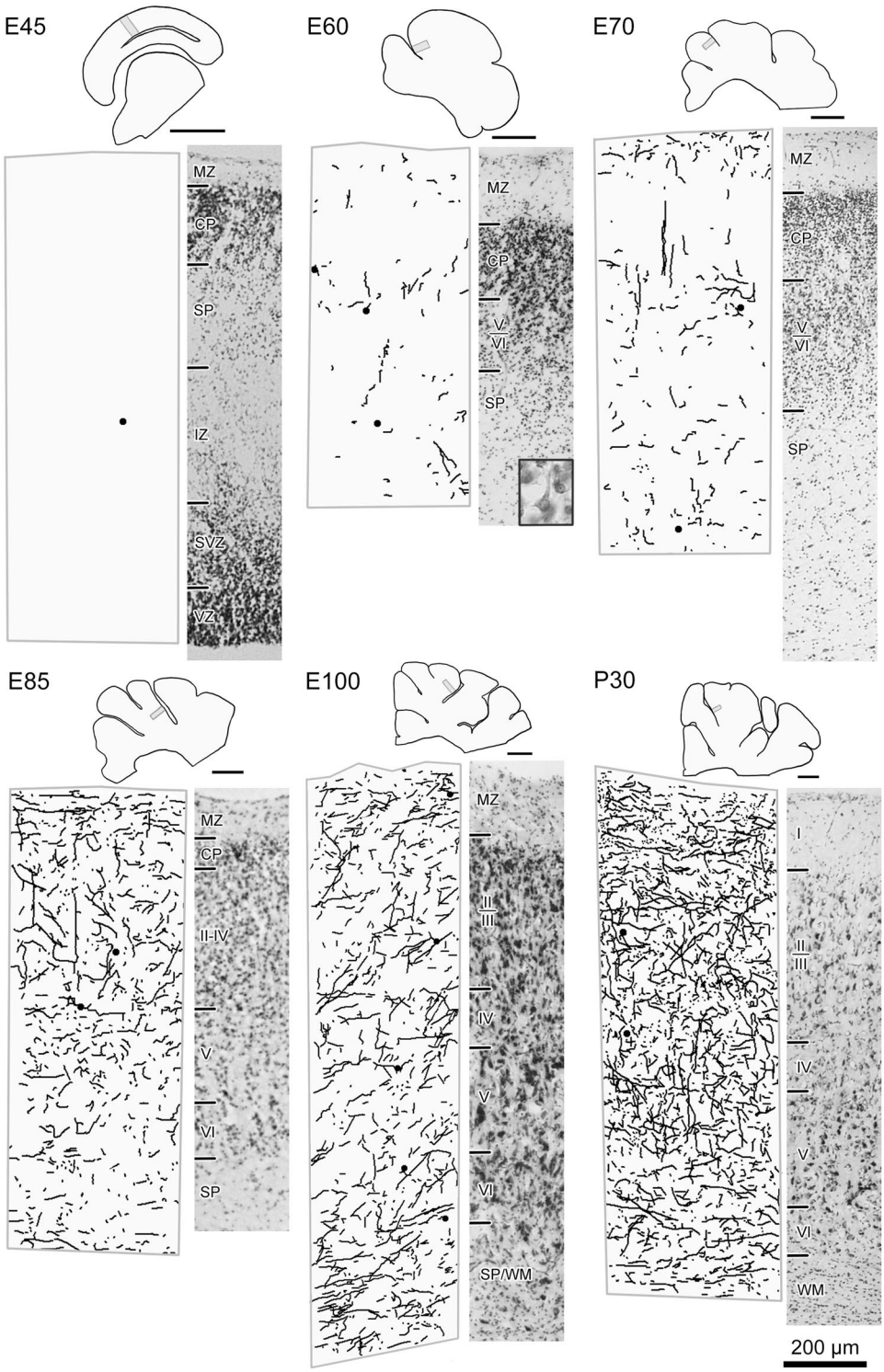

Fig. 5 Development of the axonal innervation. Panels from pia mater down to white matter are shown; large dots represent labeled somata, lines represent axons; all plotted from cryostat sections. Next to every panel, a photomicrograph from thionin-stained material has been aligned to identify the laminar compartments. In the small sketches (scale bar 3 mm, youngest stages represented larger than the older stages), rectangles indicate the position where axons were sampled. Large pyramidal neurons of layer V are identifiable by E60 (inset) and helped to delineate the layers. Scale bar 200 µm

already from E85 onwards. A dense neuropil labeling is dominant at P30. NPY-ir axons seldom pass close to other NPY-ir somata or neurites, suggesting that they do not form synapses among each other.

NPY-ir cell types

At E70 and E85, a peculiar neuron type is present in the GM just below the cell-dense cortical plate: this cell has

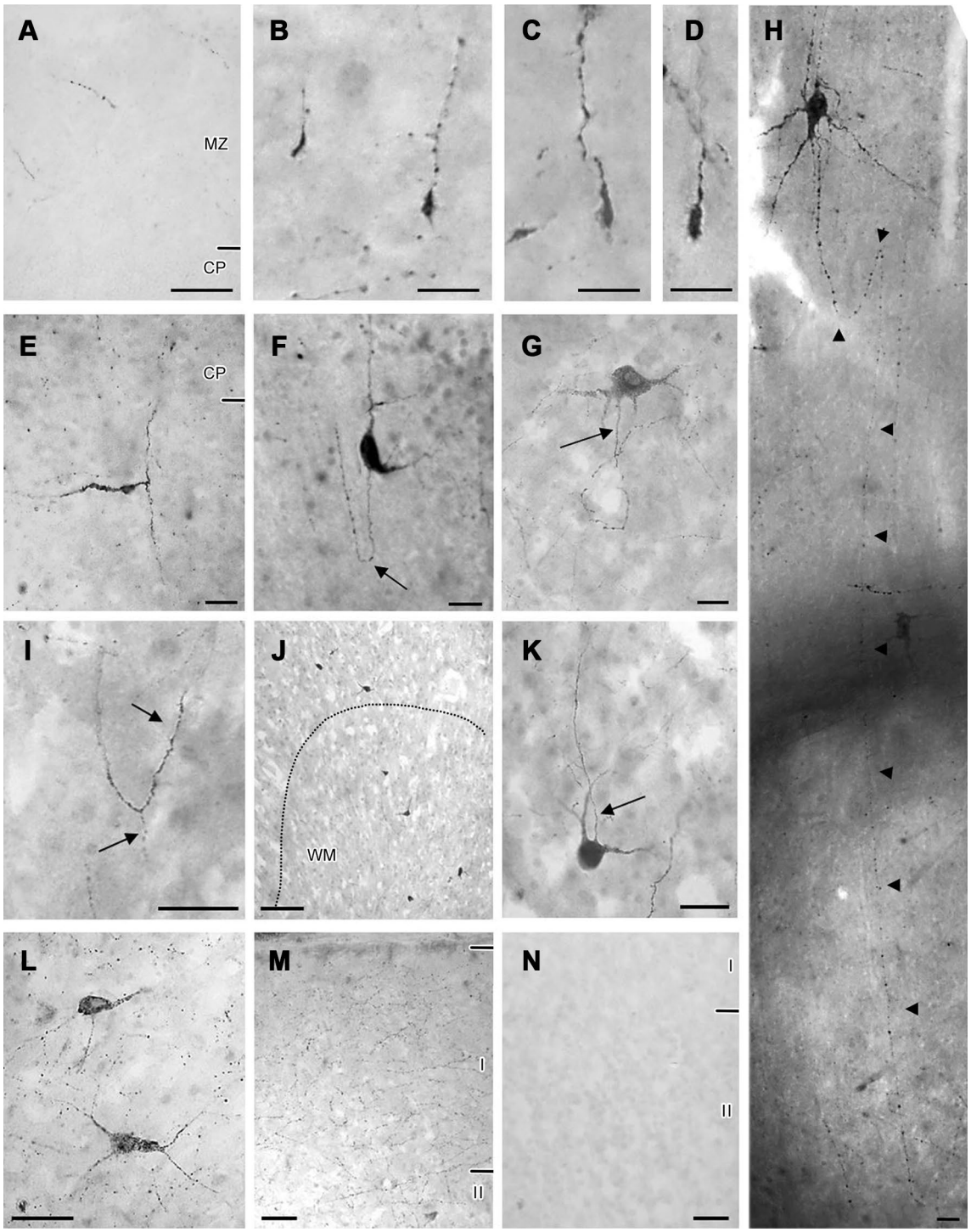

Fig. 6 Innervation and cell types. **a** Very few fibers in the marginal zone (MZ) at E60. **b–d** Axonal growth cones in GM or WM at E70, E80, E100. **e** Archaic cell with very small soma and T-branched dendrite below cortical plate (CP); E85. **f** Photomontage of axonal loop cell; **e** 70, WM. **g** Axonal loop cell; E85, WM. **h** Photomontage of axonal loop cell with long projecting axon; E85, WM. **i** Axonal loop with collateral; E100, WM. **j** Mostly intact mature somata scattering from layer V/VI down into upper WM; E100, coronal gyrus. **k** Cell in upper GM with ascending axon, E100. **l** Mature neurons in layer V/VI surrounded by plexus of varicose axons; P30. **m** Dense innervation of layer I with varicose axons; P30. **n** No staining is seen after omitting the primary antibody, here at E85, same at the other ages analyzed. Axons indicated by arrows. MZ is facing up. Scale bars 25 µm for **a, e–i, k–n**; 10 µm for **b–d**; 100 µm for **j**

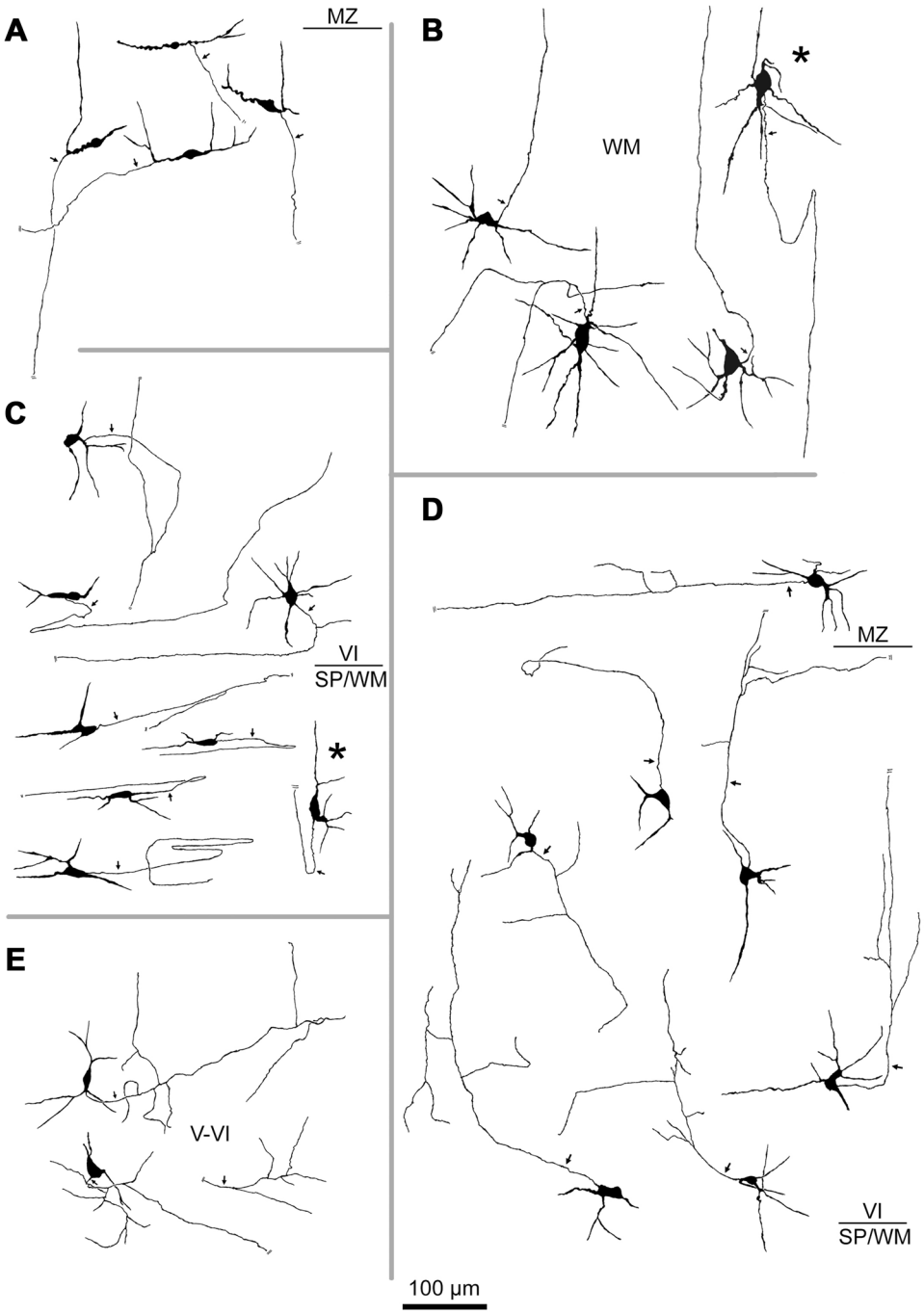

Fig. 7 NPY-ir cell types. Camera lucida drawings of fairly completely stained neurons and initial axonal patterns sampled from thick tissue slabs at E85. **a** Archaic cells of the cortical plate. **b** Axonal loop cells of the deep white matter; the four cells resided close together and are shown here with slight offset to avoid neurite overlap. **c** Axonal loop cells in layer VI and upper subplate; note the hairpin loops. **d** Neurons with vertically projecting axons resembling immature Martinotti cells. Some axons reach into the MZ. The neurons in the MZ project horizontally. **e** Neurons of layers V/VI with horizontally ramifying axons resembling basket cell projections. Laminar boundaries are indicated; MZ, marginal zone; SP, subplate. Arrows point to axons. The cells marked by asterisk are shown as photomontages in Fig. 6f, h; MZ is up

a small bipolar soma, and two thick horizontal or oblique dendrites branching in a T-shaped pattern (Figs. 6e, 7a). In keeping with previous nomenclature, we consider these cells as "archaic" neurons (Wahle and Meyer 1987). Axonal loop cells are detected in GM and SP/WM at E70, E85 and still at E100 (Figs. 6f–j, 7b, c), and they are intensely NPY-ir. Their axons can be followed for millimeters through the WM (Fig. 6h). Neurons with ascending axons (Fig. 6k) resembling Martinotti cells (Fig. 7d) are present at E85 and become prominent at E100. Other neurons at E85 and E100 already project horizontally in infragranular layers with axons resembling basket cell projections (Fig. 7e). Neurons at P30 (Fig. 6l) are multipolar, reside mainly in infragranular layers, and the staining is more punctate suggestive of NPY-ir enriched in vesicles. The neurons are surrounded by a dense plexus of varicose axons and boutons in the neuropil and numerous horizontal axons run in layer I (Fig. 6m). The WM is almost void of NPY-ir axons at P30.

NPY-ir neurons appear functional

Functionally mature neurons fire action potentials whose initiation requires an axon initial segment (AIS). To obtain data for AIS development, we co-stained for NPY and the AIS scaffold protein βIV-spectrin. βIV-spectrin was present in the axons of small immature-looking as well as mature intensely NPY-ir neurons of SP/WM and GM/MZ already at E70 (Fig. 8a–i). Axonal loop cells have an AIS as do neurons in GM at E85–E110 (Fig. 8a–d) including Martinotti neurons with ascending axons and presumptive bitufted neurons with descending axon (Fig. 8g, h, resp.). At the younger ages, AIS are short, and elongate with age (Fig. 8e, f, h).

Early on, a majority of the NPY-ir cells has the axon emanating from the soma, and nearly all have AIS residing distal to the axon's point of origin (Fig. 8i). In 6 sections at E85, 108 cells in the GM have been assessed for axon origin: 89 cells (82%) have the axon arising from the soma; 85 of them (96%) have the AIS distal with a considerable gap to the soma. Also at E85, 21 cells have been assessed in SP/WM. Here, 17 (81%) have the axon arising from the soma; and 16 of them (94%) have a distal AIS. At E110 and P30 too few cells are found in WM, and therefore all NPY-ir cells from 4 to 6 sections have been pooled. At E110, of 86 cells, 63 (73%) have axons emerging from the soma; 55 of them (87%) have a distal AIS. At P30, of 185 cells, 114 (62%) have axons emerging from the soma; 100 of them (88%) had a distal AIS (Fig. 8i). In the remaining cells at the three ages, the axons arise from dendrites, and in a majority of these cells the AIS has a clear gap to the axon's point of origin (Fig. 8f). Considering all 185 cells assessed at P30, the AIS was distal to the axon's point of origin in 87% of the neurons, irrespective of the axon's origin from the soma or from a primary or higher order dendrite. Together, from E85–P30, the proportion of distal AIS declines slightly from 96 to 88%, but the proportion of NPY-ir neurons with a somatic axon onset declined substantially from 82 to 62%.

Concurrently, the AIS itself changes. The gap between the point of origin of the axon and the βIV-spectrin-ir AIS narrows down in particular after E110 to finally 9.87 ± 3.63 µm at P30 (Online resource 8A). AIS length (mean ± SD) increases from 8.76 ± 3.42 µm at E70, to 14.79 ± 5.82 µm at E85, to 25.22 ± 7.68 µm at E110, and 26.27 ± 6.68 µm at P30 (Fig. 8i; Online resource 8B). As a reference, we have determined the length of AIS in non-NPY-ir presumably pyramidal neurons of supragranular layers around the apical parts of three gyri. Their average length (mean ± SD) is 22.51 ± 7.54 µm at E85, and thus already much longer than the AIS of NPY-ir neurons at E85. Length increases to 24.91 ± 8.04 µm at E110, and 26.55 ± 7.03 µm at P30 (Online resource 8C).

Discussion

Gyration of developing boar cortex

The nomenclature of the gyri and sulci differs in the literature, a problem rooted in the early decades of the last century. Sulcal patterns are variable between hemispheres, individuals and various breeds (Rawiel 1939), in particular the miniaturized breeds. In a dorsal view, the ansate sulcus is prominent and characteristic for the ungulate cortex (Nickel et al. 1991). The coronal sulcus branches off the ansate at its rostro-lateral bend (Campbell 1905; Brauer and Schober 1970; Minervini et al. 2016). The cruciate sulcus has been allocated to sulci at several different positions (Schmidt 2015; Bjarkam et al. 2017). We have adopted the nomenclature of Brauer and Schober (1970), who position the cruciate sulcus rostral and medial to the coronal sulcus in artiodactyles and perissodactyles, as did Craner and Ray (1991). This is in line with comparative anatomical evidence, homology principles and our own ontogenetic observations. The prominent cruciate sulcus of the boar may not be so clearly recognizable at the homologous position in domesticated or minipig breeds (Lind et al. 2007; Bjarkam et al. 2017).

Time course of NPY-ir innervation

The developmental trajectory described here for wild boar has similarities and differences to that reported for altricial species. One similarity is the turnover of transient neurons as described in cat (Wahle and Meyer 1987), human (Uylings and Delalle 1997) and rat, where cell death has been confirmed at the EM level (Valverde and Facal-Valverde 1988). Transient neurons and ontogenetic neuron death in SP and GM are well accepted. Also the MZ displays successive generations of distinct populations of Cajal-Retzius neurons (Meyer and González-Gómez 2017). The loss of SP neurons is not specific for a particular type (Arias et al. 2002). In human cortical WM, many neurons survive into adulthood (Suárez-Solá et al. 2009). A second similarity is the morphology and position of transient archaic neurons resembling those seen shortly after birth in cat (Wahle and Meyer 1987). Further, NPY-ir axonal loop cells provide a dense, transient innervation in boar, cat and human. Excitatory and peptidergic SP neurons with ascending projections are present in rat from E17–P4 (Woodhams et al. 1985), and postnatally in cat (Wahle et al. 1987; Wahle and Meyer 1987) and ferret (Kanold and Luhmann 2010). In human, NPY-ir neurons of the SP including axonal loop cells appear shortly before birth, and persist for weeks (Uylings and Delalle 1997).

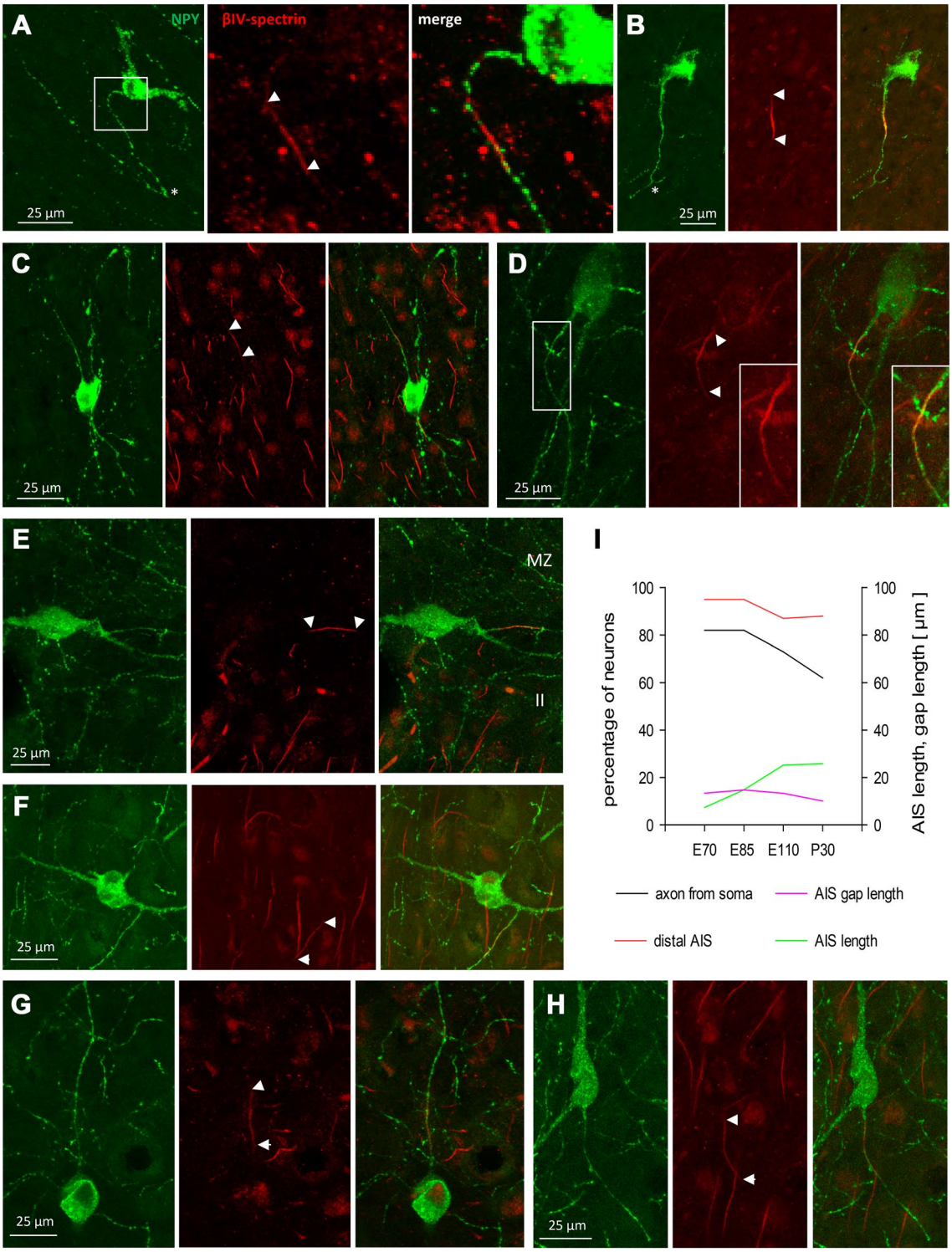

Wild boar, monkey (Mehra and Hendrickson 1993), and human (Uylings and Delalle 1997) display NPY-ir neurons in the MZ/layer I; they rarely occur in rat and cat. The major difference is the timing. In rat, cat, and monkey, the adult NPY-ir innervation pattern develops postnatally, until about P21 in rat (Woodhams et al. 1985), P50 in cat (Wahle and Meyer 1987), and even longer in macaque (Mehra and Hendrickson 1993). In wild boar, differentiated neurons with basket cell axons and Martinotti cell projections are recognizable at E85, E100, E110, overlapping with the transient innervation by SP/WM cells. Thus, in wild boar the persisting NPY-ir innervation and

◂**Fig. 8** Development of the axon initial segment of NPY-ir neurons. NPY-ir neurons (green) in GM and WM including axonal loop cells display βIV-spectrin (red) positive AIS from E70 onwards. **a, b** Axonal loop cells in SP/WM at E85; the boxed area in A is magnified to show the AIS. Asterisk indicates the loop and in **b**, the descending collateral. **c** NPY-ir neuron in GM at E85; note many rather short AIS of nearby pyramidal cells. **d** NPY-ir neuron in deep layer VI at E110. The boxed area is magnified as insets to show the alternating pattern of strong βIV-spectrin-ir and NPY-ir vesicle clusters. **e, f** NPY-ir neurons at the border of MZ and layer II at E110. Note that surrounding AIS are longer than at E85. **g** NPY-ir Martinotti neuron in layer V with ascending axon at P30. **h** NPY-ir neuron with descending axon in supragranular layers at P30. Note long AIS of neighboring pyramidal neurons. Axons arise from the soma in **a, c, d, g, h**, and from a dendrite in **b, e, f**. In A–G, the AIS are distal with a clearly visible gap to the axon's point of origin. In **h**, the AIS locates proximally and close to the axon's point of origin from the soma. All cells oriented with the MZ to the top. **i** Graphical summary of AIS development. The averages of the four parameters analyzed are plotted over age. See text and Online resource 8 for the quantitative data. AIS are delineated by arrow heads. Scale bars 25 µm

near-adult soma size form already before birth. The results suggest that the last 2–3 gestational weeks of precocial boar are equivalent to the first 1–2 postnatal weeks of altricial rodent or cat.

The subplate of the boar cortex

SP neurons are the oldest neurons generated in the cortex, since birthdating in kitten cortex revealed that many are born before midgestation (Kanold and Luhmann 2010). We found only few NPY-ir neurons below the cortical plate at E60, but plenty at E70, E85 and E100. In fetal monkey, SP neurons are co-generated and migrate with layer VI and become displaced to positions deeper than layer VI by the ingrowth of afferents (Duque et al. 2016). A similar process seems to exist in boar cortex. SP neurons establish pioneer projections to subcortical centers, provide transient synaptic support to afferents, and are the first neurons responding to sensory stimuli (Wess et al. 2017). Excitatory SP connections into the cortical plate help to wire the sensory thalamus with layer IV (Kanold and Luhmann 2010). Retrograde tracing in P28 ferret reveals cortical projections of SP neurons containing GAD, NPY, nNos and somatostatin, with a majority being glutamatergic (Finney et al. 1998). GABA-ergic neurons and connections exist in the SP, and in rodent GAD-67 colocalizes with somatostatin, which also overlaps with NPY, and with neurons expressing 5HT3aR, parvalbumin and $GABA_AR\delta$. The latter is also a marker of the numerous glutamatergic SP pyramidal neurons (Qu et al. 2016).

The role of axonal loop cells is less clear. Neurons with loop-forming axons have been observed with GAD-immunostaining in cat SP/WM leading to the assumption that NPY-ir is a co-transmitter in GABA-ergic neurons (Wahle et al. 1987). By means of their projections to the MZ, axonal loop cells have been suggested to contribute to the elimination of Cajal-Retzius neurons via GABA-mediated depolarization (Luhmann et al. 2014). Unexpectedly, we now found that the intensely SP/WM NPY-ir neurons at E85 to E110 were GAD-negative, suggesting a non-GABA-ergic phenotype for the far-projecting axonal loop cells. Furthermore, NPY-ir and GAD-ir neurons in infragranular layers and SP/WM are reciprocally wired via boutons in close apposition to somatodendritic domains as described in rodent (Kanold and Luhmann 2010; Luhmann et al. 2014). This leaves us with the following interpretations. The negative finding could be due to detection threshold. The GAD isoforms are usually co-expressed, yet, the antibody against GAD-65/67 might have failed to detect the somatodendritically enriched GAD-67 in the intensely NPY-ir neurons of SP/WM. However, GAD-65 is strongly enriched in axon terminals, and we have been unable to detect a colocalization with NPY-ir in axons and boutons in SP/WM and in the MZ as well. Thus, the neurons could be purely neuromodulatory. In fact, SP neurons richly contain rough endoplasmic reticulum suggesting a neurosecretory function (Kondo et al. 2015). Alternatively, the axonal loop cells might contain glutamate as main transmitter which could suggest an origin from the cortical VZ rather than the ganglionic eminences.

NPY is not a specific marker for inhibitory peptidergic neurons, it occurs as well in developing parvalbumin-ir cortical interneurons and pyramidal cells (Engelhardt et al. 2007). In the adult, NPY as an antiepileptic peptide cooperates with GABA to inhibit the spread of excitation (Baraban et al. 1997; Bacci et al. 2002). NPY via Y2 receptors is neuroprotective against excitotoxicity (Malva et al. 2012). In models of cellular degeneration, NPY prevents caspase activation and promotes expression of survival genes (Domin et al. 2006; Corvino et al. 2012). In the adult, infusion of NPY has also been reported to liberate glutamate via Y1 receptors (Meurs et al. 2012), and the survival-promoting action of NPY in immature rodent cerebellum is seen only with co-activation of NMDA or GABA receptors (Neveu et al. 2002). In rodent cortex, Y1-like receptors are present from birth onwards, and become highest expressed in supragranular layers and layer I, the target of axonal loop cells and the Martinotti cell innervation. Y2-like receptors are present earliest in the intermediate zone, and around birth in layers V/VI and SP (Leroux 2002). In wild boar, NPY-ir neurons and axons are in the SVZ at E70 and E85. Indeed, in the anterior SVZ of adult rodent, NPY promotes neurogenesis of granule cells via Y1/Y2 receptors (Hökfelt et al. 2008). Further, a role for NPY in enhancing neuronal migration and differentiation has been reported (Thiriet et al. 2011). NPY receptors are present presynaptically and in growth cones, and NPY elicits turning responses and enhances neurite elongation (Hökfelt et al. 2008). Together, this suggests that NPY delivered by axonal loop cells into developing GM/MZ

may has a trophic function. NPY alone or together with a main transmitter could, depending on time and layer, influence proliferation, migration and differentiation of cortical neurons besides controlling electrical activity.

Expectedly, NPY-ir neurons co-express NeuN/RBFOX3. However, they are rather weakly positive and display NeuN-ir stronger in the nucleus than in the cytosol, whereas the surrounding SP/WM and GM pyramidal neurons display a much stronger cytosolic labeling. Further, NeuN-ir seems to decrease particularly in NPY-ir neurons with signs of degeneration. Alternatively, a change in phosphorylation can render NeuN non-immunoreactive, and neuronal damage by a variety of impacts can lead to low or undetectable NeuN reactivity (Duan et al. 2016). A weak NeuN expression has been correlated with cellular immaturity in forebrain (Carter 2017), and an absence of RBFOX3 in embryonic spinal cord prevents neuronal differentiation (Kim et al. 2013). In wild boar, at E60 and E70, somata of upper layer neurons are still void of NeuN-ir because they are immature and still migratory. However, it is unlikely that the low level of NeuN in NPY-ir neurons of SP/WM at E70–E110 indicates immaturity: the entire morphology with long projections and the presence of an AIS argues against that. RBFOX3/NeuN is an important regulator for synapse formation (Wang et al. 2015). RBFOX3-negative hippocampal neurons form more excitatory synapses than wild-type neurons and among the RBFOX3-splice regulated genes are glutamate receptors and proteins enriched in synapses and AIS (Lin et al. 2016). The low expression of NeuN could suggest an enhanced ability of NPY-ir SP cells to form synapses and resulting in a stronger excitatory drive which could evoke secretion of NPY, but also the death of NPY-ir SP neurons. Alternatively, a strong excitatory drive could be causal for the low expression of NeuN. For instance, in cerebellar granule cells depolarization knocks down NeuN expression (Weyer and Schilling 2003). Similar findings have been reported for NPY-ir neurons in cortical WM in schizophrenia (Connor et al. 2011). Thus, the low level of NeuN-ir in NPY-ir SP neurons could indicate a specific functional feature.

AIS development of NPY-ir neurons

We report here for the first time on the fetal development of the AIS in a subset of interneurons. The rather low expression of NeuN/RBFOX3 in NPY-ir cells turned our focus towards AIS development because RBFOX proteins have been recently shown to govern splicing of the major AIS scaffold ankyrin-G and the assembly of the AIS in spinal motor neurons (Jacko et al. 2018). Since βIV-spectrin is bound to Ankyrin-G, its expression is restricted to AIS and nodes of Ranvier. Axons of mouse cortical neurons display ankyrin-G/βIV-spectrin-positive AIS at late prenatal ages and the AIS matures after birth in mouse visual cortex under environmental influences (Gutzmann et al. 2014). The presence of an AIS in fetal wild boar NPY-ir neurons indicates that the neurons mature quickly, assemble the AIS early, and are thus likely able to generate actions potentials as early as E70. The proportion of NPY-ir neurons with an axon arising from the soma declined during fetal development. Apparently, increasing numbers of cells appear in which the axon arises from a dendrite, either by extending it directly from the dendrite or by shifting the existing axon—either actively or passively during dendritogenesis—onto a dendrite. The incidence of distal AIS barely declines, suggesting that distal AIS are a feature common to all NPY-ir neurons, although the gap narrows down substantially until P30. In adult rodent cortex, distal AIS occur frequently in bitufted neurons and Martinotti cells (Höfflin et al. 2017). Length and position of the AIS is important for firing properties: neurons with longer and more proximal AIS usually present with higher excitability (Jamann et al. 2018). Thus, in NPY-ir neurons, the progressive AIS elongation and shift towards the soma suggest a maturation of the firing behavior. Eventually, AIS length of NPY-ir neurons equals that of supragranular pyramidal cells. Their average length was similar to values reported for adult marmoset (Atapour and Rosa 2017) and macaque monkey cortex (Sloper and Powell 1973), and slightly shorter than values of adult rodent visual cortex (Gutzmann et al. 2014). This suggests that in wild boar, AIS reach a mature length range until P30.

In summary, our study—the first of its kind in a non-domesticated, non-caged ungulate—provides evidence for a very accelerated prenatal development of the cortical NPY-ir neuron system. While the neuronal types and the transient and persisting innervation patterns are conserved across species, the time course differs. In precocial European wild boar, the adult innervation pattern develops before birth.

Materials and methods

Animal material

Fetal material was obtained via the Regionalverband Ruhr Grün from the Üfter Mark area. It derived from wild sows individually hunted for population control in accordance with the German Game Law (Jagdrecht) or killed in road accidents (see Table 1). "Young" refers to wild sows at 10–18 months of age (in German "Überläuferbachen" with first pregnancy); two sows were adult females. The Game Law requests disposal of viscera including sexual organs of wild boar as they are not permitted to enter the food chain (German Tier-LMHV § 7, Attachment Chapter III). The German Game Law permits hunting of boar piglets. In the process of evisceration, the uteri were examined for pregnancies. Fetuses were dissected from the uteri at the

Table 1 Animal material

Fetal age[a]	Date of kill	Age of wild sow	Liter size, sex	Time 1	Time 2	Organs
E35	21. 01. 2016	Young	4 (n. d.)	3 h	Processed in toto	Not prepared
E45	03. 06. 2015	Young	4 (3m, 1f)	1.5 h	4 days	Prepared
E60	25. 06. 2015	Young	5 (3m, 2f)	1 h	13 h	Prepared
E65	24. 01. 2016	Young	7 (4m, 3f)	1.5 h	15 h	Prepared
E70	08. 01. 2016	10 years	6 (4m, 2f)	4 h	10 h	Prepared
E85	22. 01. 2016	Adult	7 (2m, 5f)	1.5 h	10 h	Prepared
E100	21. 06. 2015	Young	5 (3m, 2f)	1.5 h	19 h	Prepared
E110	10. 03. 2017	Young	7 (4m, 3f)	2 h	19 h	Prepared
P30	08. 02. 2016		1 (1m)		1 h	Prepared

F, female; m, male; n.d., not determined

[a]Staged according to Henry (1968a)

Forsthof Üfter Mark, embryonic membranes were removed, and fetuses immersed in cold 4% paraformaldehyde (PFA) in 0.1M phosphate buffer pH 7.4 in tightly sealed containers, and stored in a cold place until transport to Ruhr University. Table 1 summarizes the ages and the postmortem times. Time 1 is the time until the fetuses were removed from the amniotic membranes, and immersed into fixative. Time 2 is the time period until the brains were dissected in the lab, documented, and immersed in fixative, followed by preparation of the body organs. The P30 was dissected directly after death. The ages were estimated and extrapolated by the crown–rump length and external features in comparison to published data (Henry 1968a). For older fetuses and the piglet, the tooth state was additionally taken into account. The external features are shown in Online resource 2. Birth in wild boars occurs at E114 (Henry 1968b). Brains of adult domesticated pigs were from the Institute's collection (donated 1994 by the Schlachthof Bochum, Freudenbergstraße 45, 44809 Bochum), and were immersion-fixed in phosphate-buffered 4% PFA.

Preparation and tissue processing

Fetuses were weighed and crown–rump–length was measured as straight distance from forehead to the root of the tail, and for the piglet from the tip of rostrum to the root of the tail. Animals were decapitated and body organs were prepared (see below). The E45 heads were postfixed for 4 days before brain preparation. The brains of E60 and older were immediately prepared and hemispheres were separated along the midline. The dura mater was completely removed; the pia mater was removed as completely as possible without damaging the brain. Some hemispheres were postfixed, cryoprotected and shock-frozen in isopentane-cooled on dry ice for storage in isopentane at − 80 °C. In other hemispheres, the cortex was separated from di- and mesencephalon (not done for the younger ages), and cut coronally into blocks or slabs using the coordinates indicated in Fig. 1, brain E70. Blocks were postfixed for about another 2 weeks, cryoprotected, and frozen in TissueTek for cryostat cutting. The fixative for the brains after preparation was 4% PFA in 0.1 M phosphate buffer containing 5% (vol/vol) water-saturated picric acid. Fixative was renewed once during the 2-week postfixation at 8 °C. Care was taken to position the brains such that the dorsal cortex pointed upwards to avoid squeezing of the fragile tissue. Then, the tissue blocks were immersed sequentially in 10, 17, 25% phosphate-buffered sucrose, frozen in TissueTek, and stored at − 80 °C until cutting.

Tissue blocks were equilibrated to − 20 °C, mounted into the cryostat and cut into 25-µm-thick sections (30 µm for AIS analysis), collected on coated slides (silanized slides provided better support than double-gelatinized ones), dried at 35 °C on a hot plate and stored for 1–3 days at room temperature until staining. Additionally, pieces of the pia mater were collected during brain dissection. They were handled like the brains, but were not frozen. Instead, they were stored in phosphate-buffered 25% sucrose at 4 °C with 0.002% sodium azide for free-floating whole-mount immunofluorescence staining. Further, slabs of E85 brains were thawed and 300- to 500-µm-thick sections from a gyrus were cut by hand with a razor and processed free-floating.

Immunohistochemistry on sections

Brains of both sexes were processed. Slide-mounted dried cryostat sections were encircled with a PAP pen. Sections and pieces of pia mater were washed in PB in order to remove any remaining fixative for several minutes with three changes of buffer. For antigen retrieval, sections were heated to 80 °C in citrate buffer (pH 5–6) for 40 min. After cooling down slowly over about 1 h, the sections were rinsed in TBS two times, rinsed in TBS/5% horse serum once more, and blocked for 3–5 h at room temperature in TBS/5% horse serum. Incubation in primary antibodies was started for 1 h at room temperature and continued over night at 4 °C in

moist chambers. The next day, sections were equilibrated to room temperature for 30 min, and rinsed 3 times 15 min with TBS/1% BSA.

For fluorescence staining, the autofluorescence in the sections was quenched by incubation in Sudan Black B 0.2% (w/v), dissolved in 70% isopropyl alcohol. After 45–60 min, the tissue was shortly rinsed in 70% isopropyl alcohol, equilibrated to TBS/1% BSA, and rinsed in several changes to remove the organic solvent. Afterwards, slices were incubated with ALEXA 488 and ALEXA 594-conjugated secondary antibodies for 1–2 h (see Online resource 1 for reagents). Subsequently, sections were rinsed in TBS/1% BSA 4–5 times, followed by a 5 min incubation in phosphate-buffered saline (PBS) with DAPI (1:10,000). Sections were coverslipped with Immu-Mount® (Thermo Fisher Scientific), sealed with nail polish, and stored in the dark at 8 °C until imaging.

For 3,3-diaminobenzidine (DAB) staining, sections were incubated with appropriate biotinylated secondary antibodies for 1–2 h (see Online resource 1 for reagents). Afterwards, they were rinsed 2–3 times in TBS/1% BSA, followed by a 1 h incubation in avidin-biotin-horseradish peroxidase complex. Subsequently, sections were rinsed 3 times 10 min in TBS 1% BSA and equilibrated to 0.05 M Tris buffer pH 7.4. The reaction product was developed with 0.02% DAB (Sigma Aldrich, Steinheim, Germany) in Tris buffer and 0.001% H_2O_2. Staining was stopped in Tris buffer, followed by three rinses in 0.1 M phosphate buffer pH 7.4. The DAB reaction product was intensified by incubation in 1% OsO_4 (Sigma Aldrich, Steinheim, Germany) in phosphate buffer for about 5 min. Reaction was stopped, free-floating tissue was mounted on silanized slides, dried, briefly rinsed in distilled water for desalting, dehydrated, cleared, and coverslipped with DPX (Sigma Aldrich, Steinheim, Germany). No staining was seen after omitting the primary or secondary antibodies (see Fig. 6n).

Immunohistochemistry on paraffin sections

The E35 heads in toto, hemispheres of E45, and tissue blocks of E60, E70, E85, E100 and P30 were postfixed in Bouin's fixative for about 3 weeks, embedded in paraffin and cut coronally into 10-µm-thick sections collected on silanized slides. Sections were deparaffinized, rehydrated, heated to 95 °C in 10 mM citrate buffer at pH 6 for 20 min for antigen retrieval, rinsed in Tris-buffered saline (TBS) pH 7.6, and incubated in the primary antibody against NPY (Abcam) overnight in a humid chamber. After rinsing, a biotinylated goat anti-rabbit IgG diluted at 1:200 in TBS was applied, followed by incubation with avidin–biotin complex in TBS. Bound peroxidase was revealed using 0.04% DAB, 0.05% ammonium nickel (II) sulphate, and 0.03% hydrogen peroxide in TBS pH 7.6. Sections were dehydrated, cleared, and coverslipped with Eukitt (O. Kindler, Freiburg, Germany).

Analysis

Body weight, CR-length and the weights of heart, lung, liver, gastrointestinal tract (antrum to rectum, stomach and gut not emptied), kidney and spleen were recorded and plotted over age to determine growth rates (Online resource 3). The age of the piglet was estimated P30 on the fact that the premolars P3/P4 were present in mandible and maxilla (Neef 2009).

DAB-stained material was analyzed with light microscopy. Plots of the innervation pattern were done at 400× with the Neurolucida (MicroBrightField, Inc., Williston, Vermont, USA) from 25-µm-thick frozen sections and arranged to scale. A field of interest half way up a gyrus has been selected from E60 onwards avoiding the apex and sulci, where the layers are broader and more compressed, respectively. The distribution of somata was plotted from 10-µm-thick paraffin at 400×, and plots were arranged at the same scale. The morphology of selected, fairly completely stained neurons was drawn with camera lucida at 600× with an ink fine liner from the hand-cut thick slabs, drawings were digitalized and arranged. Soma size of NPY-ir neurons was determined by sampling all intact somata (nucleus present in the plane of the section) from 25 µm cryostat section. Camera lucida drawings (1000× magnification) of the somatic outlines were digitized and somatic area in μm^2 was determined. Images were taken with a Zeiss Axiophot equipped with a CCD camera (PCO, Kelheim, Germany), some well-stained neurons were photographed through the Z-axis and the stack was assembled into a photomontage with Photoshop®; all photomontages are indicated in the figure legends. Immunofluorescence staining was analyzed with confocal microscopy with a Leica TSC SP5. We counted in confocal images from 10 arbitrarily selected ROI placed over the subplate directly adjacent to layer VI in two (E70) resp. three (E85–E110) gyri the number of NeuN-ir and NPY-ir somata (in total 2552 and 43 cells, respectively). Since NPY-ir neurons express NeuN weakly and with some even appearing void of NeuN-ir and with the observation that the very immature unipolar NPY-ir neurons were entirely void of NeuN-ir, we set the sum of NeuN-ir plus NPY-ir neurons per view field to 100%, considering only somata having the DAPI-stained nucleus in the optical plane of the confocal image. Z-stack thickness has been kept at 3.5 ± 0.5 µm for E70, and 5 ± 0.5 µm for E85–E110. The colocalization of GAD-65/67-ir and NPY-ir was done similarly at E85 placing the view fields over SP/WM.

For AIS analysis, several 30-µm sections double-stained for NPY and βIV-spectrin from E70, E85, P110/110 and P30 were analyzed and all NPY-ir neurons in SP/WM and GM/

MZ with βIV-spectrin-positive axons were imaged (Leica TSC SP5, 40× objective with 1.1 NA, 1024 × 1024 px). AIS length and gap to axon origin was measured with a previously published self-written macro using Python was used (Höfflin et al. 2017).

Acknowledgements We acknowledge the Regionalverband Ruhr, Essen, Germany, for the interest in our work. We thank Dr. Oliver Keuling, TiHo Hannover, Germany, for advice with staging. We thank Andrea Räk, Sabine Schönfelder, Christian Riedel and Silke Vorwald for technical support. This research received no specific funding.

Author contributions GM and PW conceived the experiments. CB and CB sampled the fetal material. LE, SD, JR, ME, MGG, GM and PW performed experiments or supplied tools for analysis. LE, GM and PW analyzed data and wrote the manuscript. All authors approved the manuscript.

Compliance with ethical standards

Conflict of interest The corresponding author, on behalf of the coauthors, declares no conflict of interest.

Ethical approval All applicable international, national, and/or institutional guidelines for the care and use of animals were followed. All procedures performed in studies involving animals were in accordance with the ethical standards of the institution or practice at which the studies were conducted.

References

Adrian ED (1943) Afferent areas in the brain of ungulates. Brain 66:89–103. https://doi.org/10.1093/brain/66.2.89

Andersen F, Watanabe H, Bjarkam C, Danielsen EH, Cumming P (2005) Pig brain stereotaxic standard space: mapping of cerebral blood flow normative values and effect of MPTP-lesioning. Brain Res Bull 66:17–29. https://doi.org/10.1016/j.brainresbull.2005.02.033

Arias MS, Baratta J, Yu J, Robertson RT (2002) Absence of selectivity in the loss of neurons from the developing cortical subplate of the rat. Dev Brain Res 139:331–335

Atapour N, Rosa MGP (2017) Age-related plasticity of the axon initial segment of cortical pyramidal cells in marmoset monkeys. Neurobiol Aging 57:95–103. https://doi.org/10.1016/j.neurobiolaging.2017.05.013

Bacci A, Huguenard JR, Prince DA (2002) Differential modulation of synaptic transmission by neuropeptide Y in rat neocortical neurons. Proc Natl Acad Sci U S A 99:17125–17130. https://doi.org/10.1073/pnas.012481899

Baker EW, Platt SR, Lau VW, Grace HE, Holmes SP, Wang L, Duberstein KJ, Howerth EW, Kinder HA, Stice SL, Hess DC, Mao H, West FD (2017) Induced pluripotent stem cell-derived neural stem cell therapy enhances recovery in an ischemic stroke pig model. Sci Rep 7:10075. https://doi.org/10.1038/s41598-017-10406-x

Baraban SC, Hollopeter G, Erickson JC, Schwartzkroin PA, Palmiter RD (1997) Knock-out mice reveal a critical antiepileptic role for neuropeptide Y. J Neurosci 17:8927–8936

Bjarkam CR, Glud AN, Orlowski D, Sørensen JCH, Palomero-Gallagher N (2017) The telencephalon of the Göttingen minipig, cytoarchitecture and cortical surface anatomy. Brain Struct Funct 222:2093–2114. https://doi.org/10.1007/s00429-016-1327-5

Böndel JC (2017) Vergleichende morphometrische Untersuchungen am Gehirn von *Sus scrofa* und *Sus scrofa* f. domestica. Dissertation, Tierärztliche Fakultät, Ludwig-Maximilians-Universität München. http://edoc.ub.uni-muenchen.de:21069, https://edoc.ub.uni-muenchen.de/21069/

Brauer K, Schober W (1970) Katalog der Säugetiergehirne: catalogue of mammalian brains. VEB Gustav Fischer Verlag, Jena

Campbell AW (1905) Histological studies on the localisation of cerebral function. Cambridge University Press, Cambridge

Carter DA (2017) Molecular phenotyping of transient postnatal tyrosine hydroxylase neurons in the rat bed nucleus of the stria terminalis. J Chem Neuroanat 82:29–38. https://doi.org/10.1016/j.jchemneu.2017.04.002

Connor CM, Crawford BC, Akbarian S (2011) White matter neuron alterations in schizophrenia and related disorders. Int J Dev Neurosci 29:325–334. https://doi.org/10.1016/j.ijdevneu.2010.07.236

Conrad MS, Sutton BP, Dilger RN, Johnson RW (2014) An in vivo three-dimensional magnetic resonance imaging-based averaged brain collection of the neonatal piglet (*Sus scrofa*). PLoS One 9:e107650. https://doi.org/10.1371/journal.pone.0107650

Corvino V, Marchese E, Giannetti S, Lattanzi W, Bonvissuto D, Biamonte F, Mongiovì AM, Michetti F, Geloso MC (2012) The neuroprotective and neurogenic effects of neuropeptide Y administration in an animal model of hippocampal neurodegeneration and temporal lobe epilepsy induced by trimethyltin. J Neurochem 122:415–426. https://doi.org/10.1111/j.1471-4159.2012.07770.x

Craner SL, Ray RH (1991) Somatosensory cortex of the neonatal pig: I. Topographic organization of the primary somatosensory cortex (SI). J Comp Neurol 306:24–38. https://doi.org/10.1002/cne.903060103

Dilger RN, Johnson RW (2010) Behavioral assessment of cognitive function using a translational neonatal piglet model. Brain Behav Immun 24:1156–1165. https://doi.org/10.1016/j.bbi.2010.05.008

Domin H, Kajta M, Smiałowska M (2006) Neuroprotective effects of MTEP, a selective mGluR5 antagonists and neuropeptide Y on the kainate-induced toxicity in primary neuronal cultures. Pharmacol Rep 58:846–858

Duan W, Zhang Y-P, Hou Z, Huang C, Zhu H, Zhang C-Q, Yin Q (2016) Novel insights into NeuN: from neuronal marker to splicing regulator. Mol Neurobiol 53:1637–1647. https://doi.org/10.1007/s12035-015-9122-5

Duque A, Krsnik Z, Kostović I, Rakic P (2016) Secondary expansion of the transient subplate zone in the developing cerebrum of human and nonhuman primates. Proc Natl Acad Sci USA 113:9892–9897. https://doi.org/10.1073/pnas.1610078113

Engelhardt M, Di Cristo G, Berardi N, Maffei L, Wahle P (2007) Differential effects of NT-4, NGF and BDNF on development of neurochemical architecture and cell size regulation in rat visual cortex during the critical period. Eur J Neurosci 25:529–540. https://doi.org/10.1111/j.1460-9568.2006.05301.x

Finney EM, Stone JR, Shatz CJ (1998) Major glutamatergic projection from subplate into visual cortex during development. J Comp Neurol 398:105–118. https://doi.org/10.1002/(SICI)1096-9861(19980817)398:1%3C105:AID-CNE7%3E3.0.CO;2-5

Friel M, Kunc HP, Griffin K, Asher L, Collins LM (2016) Acoustic signalling reflects personality in a social mammal. R Soc Open Sci 3:160178. https://doi.org/10.1098/rsos.160178

Fulgione D, Trapanese M, Buglione M, Rippa D, Polese G, Maresca V, Maselli V (2017) Pre-birth sense of smell in the wild boar: the ontogeny of the olfactory mucosa. Zoology (Jena) 123:11–15. https://doi.org/10.1016/j.zool.2017.05.003

Gieling ET, Nordquist RE, van der Staay FJ (2011) Assessing learning and memory in pigs. Anim Cogn 14:151–173. https://doi.org/10.1007/s10071-010-0364-3

Grate LL, Golden JA, Hoopes PJ, Hunter JV, Duhaime A-C (2003) Traumatic brain injury in piglets of different ages: techniques for

lesion analysis using histology and magnetic resonance imaging. J Neurosci Methods 123:201–206. https://doi.org/10.1016/S0165-0270(02)00361-8

Gutzmann A, Ergül N, Grossmann R, Schultz C, Wahle P, Engelhardt M (2014) A period of structural plasticity at the axon initial segment in developing visual cortex. Front Neuroanat 8:11. https://doi.org/10.3389/fnana.2014.00011

Hamel E (2006) Perivascular nerves and the regulation of cerebrovascular tone. J Appl Physiol 100:1059–1064. https://doi.org/10.1152/japplphysiol.00954.2005

Henry VG (1968a) Fetal development in European Wild Hogs. J Wildl Manag 32:966. https://doi.org/10.2307/3799577

Henry VG (1968b) Length of Estrous cycle and gestation in European Wild Hogs. J Wildl Manag 32:406. https://doi.org/10.2307/3798986

Höfflin F, Jack A, Riedel C, Mack-Bucher J, Roos J, Corcelli C, Schultz C, Wahle P, Engelhardt M (2017) Heterogeneity of the axon initial segment in interneurons and pyramidal cells of rodent visual cortex. Front Cell Neurosci 11:332. https://doi.org/10.3389/fncel.2017.00332

Hökfelt T, Stanic D, Sanford SD, Gatlin JC, Nilsson I, Paratcha G, Ledda F, Fetissov S, Lindfors C, Herzog H, Johansen JE, Ubink R, Pfenninger KH (2008) NPY and its involvement in axon guidance, neurogenesis, and feeding. Nutrition 24:860–868. https://doi.org/10.1016/j.nut.2008.06.010

Holm IE, Alstrup AKO, Luo Y (2016) Genetically modified pig models for neurodegenerative disorders. J Pathol 238:267–287. https://doi.org/10.1002/path.4654

Jacko M, Weyn-Vanhentenryck SM, Smerdon JW, Yan R, Feng H, Williams DJ, Pai J, Xu K, Wichterle H, Zhang C (2018) Rbfox splicing factors promote neuronal maturation and axon initial segment assembly. Neuron. https://doi.org/10.1016/j.neuron.2018.01.020

Jamann N, Jordan M, Engelhardt M (2018) Activity-dependent axonal plasticity in sensory systems. Neuroscience 368:268–282. https://doi.org/10.1016/j.neuroscience.2017.07.035

Kanold PO, Luhmann HJ (2010) The subplate and early cortical circuits. Annu Rev Neurosci 33:23–48. https://doi.org/10.1146/annurev-neuro-060909-153244

Kawamura K, Sakata N, Takebayashi S (1991) Neuropeptide Y- and vasoactive intestinal polypeptide-containing nerve fibers in the human cerebral arteries: characteristics of distribution. Angiology 42:35–43. https://doi.org/10.1177/000331979104200106

Kim KK, Nam J, Mukouyama Y-S, Kawamoto S (2013) Rbfox3-regulated alternative splicing of Numb promotes neuronal differentiation during development. J Cell Biol 200:443–458. https://doi.org/10.1083/jcb.201206146

Klassen H, Kiilgaard JF, Warfvinge K, Samuel MS, Prather RS, Wong F, Petters RM, La Cour M, Young MJ (2012) Photoreceptor differentiation following transplantation of allogeneic retinal progenitor cells to the dystrophic rhodopsin Pro347Leu transgenic pig. Stem Cells Int 2012:939801. https://doi.org/10.1155/2012/939801

Kondo S, Al-Hasani H, Hoerder-Suabedissen A, Wang WZ, Molnár Z (2015) Secretory function in subplate neurons during cortical development. Front Neurosci 26:9:100. https://doi.org/10.3389/fnins.2015.00100

Kruska D (1970) Vergleichend cytoarchitektonische Untersuchungen an Gehirnen von Wild- und Hausschweinen. Z Anat Entwickl Gesch 131:291–324. https://doi.org/10.1007/BF00519973

Lahvis GP (2017) Unbridle biomedical research from the laboratory cage. Elife. https://doi.org/10.7554/eLife.27438

Leroux P (2002) Localization and characterization of NPY/PYY receptors in rat frontoparietal cortex during development. J Comp Neurol 442:35–47. https://doi.org/10.1002/cne.1420

Lin Y-S, Wang H-Y, Huang D-F, Hsieh P-F, Lin M-Y, Chou C-H, Wu I-J, Huang G-J, Gau SS-F, Huang H-S (2016) Neuronal splicing regulator RBFOX3 (NeuN) regulates adult hippocampal neurogenesis and synaptogenesis. PLoS One 11:e0164164. https://doi.org/10.1371/journal.pone.0164164

Lind NM, Moustgaard A, Jelsing J, Vajta G, Cumming P, Hansen AK (2007) The use of pigs in neuroscience: modeling brain disorders. Neurosci Biobehav Rev 31:728–751. https://doi.org/10.1016/j.neubiorev.2007.02.003

Luhmann HJ, Kirischuk S, Sinning A, Kilb W (2014) Early GABAergic circuitry in the cerebral cortex. Curr Opin Neurobiol 26:72–78. https://doi.org/10.1016/j.conb.2013.12.014

Malva JO, Xapelli S, Baptista S, Valero J, Agasse F, Ferreira R, Silva AP (2012) Multifaces of neuropeptide Y in the brain–neuroprotection, neurogenesis and neuroinflammation. Neuropeptides 46:299–308. https://doi.org/10.1016/j.npep.2012.09.001

Markram H, Toledo-Rodriguez M, Wang Y, Gupta A, Silberberg G, Wu C (2004) Interneurons of the neocortical inhibitory system. Nat Rev Neurosci 5:793–807. https://doi.org/10.1038/nrn1519

McGowan JE, Haynes-Laing AG, Mishra OP, Delivoria-Papadopoulos M (1995) The effect of acute hypoglycemia on the cerebral NMDA receptor in newborn piglets. Brain Res 670:283–288. https://doi.org/10.1016/0006-8993(94)01289-T

Mc-Phearson-McCassidy RL (2003) Fetal growth and development of the pig. M.Sc. Thesis, Texas Tech University. http://hdl.handle.net/2346/8522

Mehra RD, Hendrickson AE (1993) A comparison of the development of neuropeptide and MAP2 immunocytochemical labeling in the macaque visual cortex during pre- and postnatal development. J Neurobiol 24:101–124. https://doi.org/10.1002/neu.480240109

Meurs A, Portelli J, Clinckers R, Balasubramaniam A, Michotte Y, Smolders I (2012) Neuropeptide Y increases in vivo hippocampal extracellular glutamate levels through Y1 receptor activation. Neurosci Lett 510:143–147. https://doi.org/10.1016/j.neulet.2012.01.023

Meyer G, González-Gómez M (2017) The subpial granular layer and transient versus persisting Cajal–Retzius neurons of the fetal human cortex. Cereb Cortex. https://doi.org/10.1093/cercor/bhx110

Minervini S, Accogli G, Pirone A, Graïc J-M, Cozzi B, Desantis S (2016) Brain mass and encephalization quotients in the domestic industrial pig (*Sus scrofa*). PLoS One 11:e0157378. https://doi.org/10.1371/journal.pone.0157378

Mudd AT, Dilger RN (2017) Early-life nutrition and neurodevelopment: use of the piglet as a translational model. Adv Nutr 8:92–104. https://doi.org/10.3945/an.116.013243

Neef J (2009) Untersuchungen zur Reproduktionsdynamik beim mitteleuropäischen Wildschwein, Edition scientifique, 1 Aufl. VVB Laufersweiler, Giessen

Neveu I, Rémy S, Naveilhan P (2002) The neuropeptide Y receptors, Y1 and Y2, are transiently and differentially expressed in the developing cerebellum. Neuroscience 113:767–777. https://doi.org/10.1016/S0306-4522(02)00256-7

Nickel R, Schummer A, Seiferle E (1991) Lehrbuch der Anatomie der Haustiere. B and IV: Nervensystem, Sinnesorgane, Endokrine Drüsen. Parey, Berlin

Nielsen KB, Søndergaard A, Johansen MG, Schauser K, Vejlsted M, Nielsen AL, Jørgensen AL, Holm IE (2010) Reelin expression during embryonic development of the pig brain. BMC Neurosci 11:75. https://doi.org/10.1186/1471-2202-11-75

Pond WG, Boleman SL, Fiorotto ML, Ho H, Knabe DA, Mersmann HJ, Savell JW, Su DR (2000) Perinatal ontogeny of brain growth in the domestic pig. Proc Soc Exp Biol Med 223:102–108. https://doi.org/10.1046/j.1525-1373.2000.22314.x

Qu G-J, Ma J, Yu Y-C, Fu Y (2016) Postnatal development of GABAergic interneurons in the neocortical subplate of mice. Neuroscience 322:78–93. https://doi.org/10.1016/j.neuroscience.2016.02.023

Rawiel F (1939) Untersuchungen an Hirnen von Wild- und Hausschweinen. Z Anat Entwickl Gesch 110:344–370. https://doi.org/10.1007/BF02118790

Saikali S, Meurice P, Sauleau P, Eliat P-A, Bellaud P, Randuineau G, Vérin M, Malbert C-H (2010) A three-dimensional digital segmented and deformable brain atlas of the domestic pig. J Neurosci Methods 192:102–109. https://doi.org/10.1016/j.jneumeth.2010.07.041

Sakoh M, Ostergaard L, Gjedde A, Røhl L, Vestergaard-Poulsen P, Smith DF, Le Bihan D, Sakaki S, Gyldensted C (2001) Prediction of tissue survival after middle cerebral artery occlusion based on changes in the apparent diffusion of water. J Neurosurg 95:450–458. https://doi.org/10.3171/jns.2001.95.3.0450

Sauleau P, Lapouble E, Val-Laillet D, Malbert C-H (2009) The pig model in brain imaging and neurosurgery. Animal 3:1138–1151. https://doi.org/10.1017/S1751731109004649

Schmidt V (2015) Comparative anatomy of the pig brain: an integrative magnetic resonance imaging (MRI) study of the porcine brain with special emphasis on the external morphology of the cerebral cortex, 1. Aufl. Edition scientifique. Laufersweiler, Giessen

Sloper JJ, Powell TPS (1973) Observations on the axon initial segment and other structures in the neocortex using conventional staining and ethanolic phosphotungstic acid. Brain Res 50:163–169. https://doi.org/10.1016/0006-8993(73)90602-1

Smith DH, Chen X-H, Nonaka M, Trojanowski JQ, Lee V-Y, Saatman KE, Leoni MJ, Xu B-N, Wolf JA, Meaney DF (1999) Accumulation of amyloid β and tau and the formation of neurofilament inclusions following diffuse brain injury in the pig. J Neuropathol Exp Neurol 58:982–992. https://doi.org/10.1097/00005072-199909000-00008

Suárez-Solá ML, González-Delgado FJ, Pueyo-Morlans M, Medina-Bolívar OC, Hernández-Acosta NC, González-Gómez M, Meyer G (2009) Neurons in the white matter of the adult human neocortex. Front Neuroanat 3:7. https://doi.org/10.3389/neuro.05.007.2009

Sweasey D, Patterson DSP, Glancy EM (1976) Biphasic myelination and the fatty acid composition of cerebrosides and cholesterol esters in the developing central nervous system of the domestic pig. J Neurochem 27:375–380. https://doi.org/10.1111/j.1471-4159.1976.tb12256.x

Thiriet N, Agasse F, Nicoleau C, Guégan C, Vallette F, Cadet J-L, Jaber M, Malva JO, Coronas V (2011) NPY promotes chemokinesis and neurogenesis in the rat subventricular zone. J Neurochem 116:1018–1027. https://doi.org/10.1111/j.1471-4159.2010.07154.x

Uylings H, Delalle I (1997) Morphology of neuropeptide Y-immunoreactive neurons and fibers in human prefrontal cortex during prenatal and postnatal development. J Comp Neurol. https://doi.org/10.1002/(SICI)1096-9861(19970324)379:43.0.CO;2-4

Valverde F, Facal-Valverde MV (1988) Postnatal development of interstitial (subplate) cells in the white matter of the temporal cortex of kittens: a correlated Golgi and electron microscopic study. J Comp Neurol 269:168–192. https://doi.org/10.1002/cne.902690203

Veit A, Wondrak M, Huber L (2017) Object movement re-enactment in free-ranging Kune Kune piglets. Anim Behav 132:49–59. https://doi.org/10.1016/j.anbehav.2017.08.004

Vodicka P, Smetana K, Dvoránková B, Emerick T, Xu YZ, Ourednik J, Ourednik V, Motlík J (2005) The miniature pig as an animal model in biomedical research. Ann N Y Acad Sci 1049:161–171. https://doi.org/10.1196/annals.1334.015

Wahle P, Meyer G (1987) Morphology and quantitative changes of transient NPY-ir neuronal populations during early postnatal development of the cat visual cortex. J Comp Neurol 261:165–192. https://doi.org/10.1002/cne.902610202

Wahle P, Meyer G, Albus K (1986) Localization of NPY-immunoreactivity in the cat's visual cortex. Exp Brain Res 61:364–374

Wahle P, Meyer G, Wu J-Y, Albus K (1987) Morphology and axon terminal pattern of glutamate decarboxylase-immunoreactive cell types in the white matter of the cat occipital cortex during early postnatal development. Dev Brain Res 36:53–61. https://doi.org/10.1016/0165-3806(87)90064-2

Wang H-Y, Hsieh P-F, Huang D-F, Chin P-S, Chou C-H, Tung C-C, Chen S-Y, Lee L-J, Gau SS-F, Huang H-S (2015) RBFOX3/NeuN is required for hippocampal circuit balance and function. Sci Rep 5:17383. https://doi.org/10.1038/srep17383

Wess JM, Isaiah A, Watkins PV, Kanold PO (2017) Subplate neurons are the first cortical neurons to respond to sensory stimuli. Proc Natl Acad Sci USA 114:12602–12607. https://doi.org/10.1073/pnas.1710793114

Weyer A, Schilling K (2003) Developmental and cell type-specific expression of the neuronal marker NeuN in the murine cerebellum. J Neurosci Res 73:400–409. https://doi.org/10.1002/jnr.10655

Woodhams PL, Allen YS, McGovern J, Allen JM, Bloom SR, Balazs R, Polak JM (1985) Immunohistochemical analysis of the early ontogeny of the neuropeptide Y system in rat brain. Neuroscience 15:173–202

Yue X, Mehmet H, Penrice J, Cooper C, Cady E, Wyatt JS, Reynolds EOR, Edwards AD, Squier MV (1997) Apoptosis and necrosis in the newborn piglet brain following transient cerebral hypoxia–ischaemia. Neuropathol Appl Neurobiol 23:16–25. https://doi.org/10.1111/j.1365-2990.1997.tb01181.x